Physica Medica 65 (2019) 150–156

Contents lists available at ScienceDirect

Physica Medica

journal homepage: www.elsevier.com/locate/ejmp

Original paper

Improving bleeding detector features for electron intraoperative radiotherapy

Enrique Sanchis[a,d,*], Silvia Casans[a], Rafael García-Gil[a], Julio Martos[a], Enrique Sanchis-Sánchez[b,d], Ignacio Pérez-Calatayud[a], María José Pérez-Calatayud[c], José Pérez-Calatayud[c,d]

[a] Department of Electronic Engineering, University of Valencia, E-46100, Spain
[b] Department of Physical Therapy, University of Valencia, E-46010, Spain
[c] Department of Radiation Oncology, La Fe Polytechnic and University Hospital, Valencia E-46026, Spain
[d] IRIMED Joint Research Unit (IIS La Fe – UV), Valencia, Spain

ARTICLE INFO

Keywords:
Intraoperative radiotherapy
Bleeding
Electrons
Capacitive sensor

ABSTRACT

Purpose: The aim of this work is to improve the potential bleeding detection during intraoperative radiotherapy with linac polymethyl methacrylate applicators (PMMA), based on one previously developed. The improvements carried out have been focused on: i) minimizing the impact of the detector on the visual through the plastic applicators and ii) avoiding the asymmetry in the detection capability when the applicator is tilted.
Methods: Simulations have been made to select the geometry that provides a reduced visual impact on the applicator as well as allowing an independent response with the tilting angle of the applicator. A low-noise circuit for signal conditioning has been developed. Measurements have been made on three setups: 10 cm, 7 cm and 4 cm applicator diameters, 0° and 45° tilted.
Results: The detector has a visibility through the applicator greater than 50%. Due to the geometry, optimal detection is ensured regardless of its orientation when the applicator is tilted. It is possible to detect the presence of fluid well below the typical perturbing fluid depth established by the clinic (1–1.5 cm).
Conclusions: The detector can distinguish the presence of around 0.5 cm of fluid depth while showing a high visual field through the PMMA applicators and providing a measure that does not depend on the detector orientation when the applicator is tilted. The prototype is ready for its industrialization by embedding it into the applicator for clinical use. The detector would have a significant impact on both the quality assurance and the outcome of the treatment.

1. Introduction

Intraoperative electron beam radiation therapy (IOERT) allows the precise delivery of high-dose electron beam radiation at the time of surgery, being the target the residual tumor or its bed, sparing the dose on surround healthy tissues [1]. The procedure involves delivery of a single-fraction high dose being the radiation collimated by a specific applicator. IOERT can improve the therapeutic index, as it enables direct visualization and more accurate mapping of the target area, thus improving local control of the tumor [2–9]. Moreover, shielding or removal of adjacent tissues and organs makes it possible to increase the dose on the target areas while minimizing the risk of irradiating critical structures.

In this technique, one of the potential uncertainties or dose misadministration events is the potential bleeding in the post-resected surface [10], that can be especially critical in high-vascularized scenarios or in presence of organic fluids. In fact, it was evidenced in the in vivo experimental study of Lopez-Tarjuelo et al. [11] in which they faced with significant deviations due to the blood presence. We ourselves have faced with very vascularized scenarios in some sarcomas or pelvic recurrence cases, so frequent suction was required to keep it free of fluids without having the complete guarantee that this situation is maintained along all the irradiation procedure.

In our opinion, the possibility of fluid detection into the applicator during IOERT will have a significant impact both in quality assurance and outcome of treatment. With regard to quality, the improvement is because we assure that the irradiation has been carried out in a foreseen manner, avoiding serious errors due to variations in the irradiation

* Corresponding author at: Department of Electronic Engineering, University of Valencia, E-46100, Spain.
E-mail address: enrique.sanchis@uv.es (E. Sanchis).

https://doi.org/10.1016/j.ejmp.2019.08.015
Received 4 June 2019; Received in revised form 22 July 2019; Accepted 23 August 2019
Available online 29 August 2019

depth due to the presence of fluids. As regards the outcome of treatment, the improvement is because there is a right correlation between administered dose and results.

In order to monitor the possible bleeding or presence of organic fluids in the post-resected surface during the intraoperative radiotherapy treatment, a yes/no detector prototype based on a capacitive sensor was proposed by Sanchis et al. [12]. The detector was designed under the premise of extreme simplicity, bearing in mind a possible integration of the detector into the LIAC HWL applicator itself [13]. On the one hand, in order to obtain enough sensitivity, the chosen geometry was the one that maximized the variations of the capacitance, implemented with two continuous copper strips surrounding the 2 cm lower part of the applicator and covering almost the entire perimeter of the applicator, except two gaps of 0.5 cm between the two conductors. On the other hand, a simple readout circuit based on a RC network was chosen, in which C is the equivalente capacitance of the bleeding detector and the resistor R the only external element.

The possible interference between the electromagnetic fields due to the accelerator and the capacitive detector was evaluated in Sanchis et al. [12]. In no case any alteration was observed, neither in the operation of the detector nor in the accelerator.

Although the acceptance of the detector has been satisfactory, feedback from the clinic provides some remarks that could led to improvements. On the one hand, because as expressed by Nevelsky et al. [14], "PMMA applicators offer the advantage of being transparent compared to metallic applicators, which makes positioning of the applicator in the patient comfortable for the surgeon", it is convenient that the detector does not compromise significantly the visual through the applicator. Even if the perturbation on visibility of the previously designed detector was low and circumscribed to the border of the applicator, with the new design we aim to even improve the visibility. On the other hand, its inherent geometry would cause an asymmetry in the detection when the applicator is tilted thus producing errors in the determination of the fluid depth into the applicator. Even if literature has established significative values of 1–1.5 cm as typical perturbating fluid depth for producing potential uncertainties or dose misadministration's events [15], in this work we have considered 0.5 cm as an ideal limit to be detected as we already previously established in [12].

Therefore, the aim of this work is to modify the sensor geometry of the previously designed one thus providing a sufficient visual field through the PMMA applicator while ensuring optimal detection regardless of the orientation when the applicator is tilted. The goal of obtaining the ideal detection limit is maintained.

2. Matherial and methods

2.1. Sensor description

We propose a capacitive sensor which is a modification of the one presented in Sanchis et al. [12]. The proposed new geometry is based on two capacitive plates, each one formed by a set of strips. The strips of each plate are interspersed with each other, as shown in Fig. 1. This arrangement should reduce the effects of the asymmetry in the distribution of the fluid to be detected regardless the different orientations of the applicator when it is tilted as well as permitting a high lateral visibility.

The capacitive sensor is then based on the modification of the relative permitivity of the space affected by the electric field created by the two plates when polarized. The shape adopted by the fluid when filling the applicator will define the variation of the detector capacity.

2.2. Geometry simulations

Simulations have been carried out in Comsol Mutiphysics [16] to obtain the capacitance of the sensor for different fluid volumes for different geometries, when the distribution of the surface of the capacitor plates is modified. Two sets of simulations using the 7 cm diameter applicator have been carried out (it should be noted that for the purpose of the simulations the choice of one diameter or another turns out to be irrelevant). The first one corresponds to the geometry used in our previously designed detector [12] with the non beveled applicator placed in different tilting angles (i.e. vertical and 45° tilted) and different orientations when tilted, while the second one shows the expected response for the newly designed detector, again for the same orientations of the applicator. A visibility through the sensor strips higher than 50% has been considered. Table 1 summarizes the conditions of the simulated model.

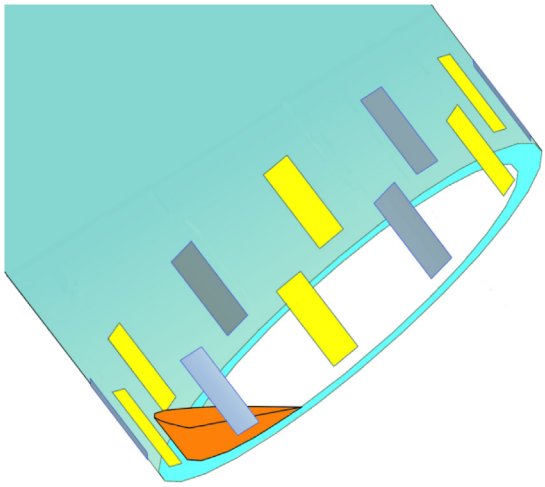

Fig. 1. Distribution of the two sets of facing strips forming the two plates. Yellow: top strips; grey: bottom strips; orange: volume of fluid to be detected in the worst scenario with extreme tilt in which the fluid is accumulated in a corner, occupying a small fraction of the applicator surface. (For interpretation of the references to colour in this figure legend, the reader is referred to the web version of this article.)

Fig. 2 shows the simulated capacitance vs. fluid depth (up to 1.8 cm), measured with respect to the horizontal surface, for both sets of simulations: Fig. 2a shows the simulation results obtained for the previously designed detector (two quasi-continuous strips forming the two plates) while Fig. 2b shows the simulation results for the newly detector with the proposed geometry as shown in Fig. 1.

As shown in Fig. 2a, the sensitivity of the previous sensor was high (i.e. 0.217 pF/mm) when the applicator is located in vertical position (blue line) but it is significantly reduced when it is 45° tilted (red and yellow lines), its value depending on whether the orientation of the fluid is towards the gap between the two strips (i.e. 0.056 pF/mm; 45° (I) in red), or towards the center of one of the two strips (i.e. 0.004 pF/mm; 45° (II) in yellow).

However, according to Fig. 2b, with the new geometry a sensitivity of 0.054 pF/mm is obtained when the applicator is located in a vertical position and 0.015 pF/mm when it is 45° tilted, regardless of the orientation of the fluid, either towards the separation between two strips or towards the center of one strip. Therefore, the orientation dependence is practically eliminated with the proposed geometry. However, the sensitivity has been considerably reduced, so it must be recovered by modifying the measurement procedure by means of an improved low noise reading circuit based on a differential measurement.

Finally, it is worth noticing that other conductor materials have been also considered for the implementation of the detector; among them, aluminum was particularly studied for its easier use and lower implementation costs compared to others. Simulations using aluminum-based strips are practically identical than for copper-based strips, so that copper has been chosen for the detector because its simplicity of manufacturing.

Table 1
Parameters used for the simulated model corresponding to the proposed geometry.

	Diameter (mm)		Material	Relative permittivity (ε)
	Outer	Inner		
Applicator	80	70	Methacrylate	3.6

	Visual	Plate height (mm)	Plate width (mm)	Material	Strips	Distance to the bottom surface (mm)
Capacitor	> 66%	15	5	Cu	12	3

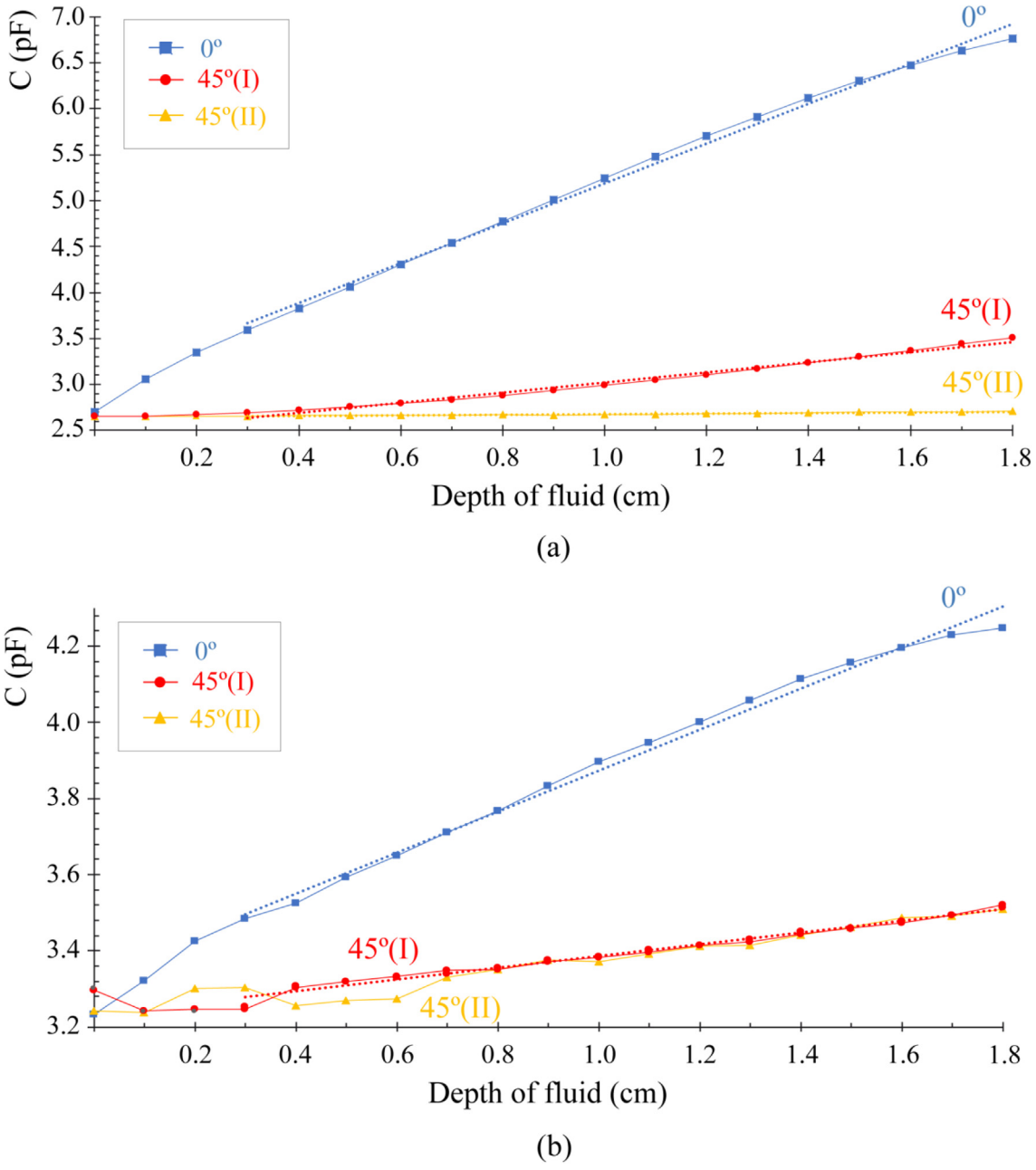

Fig. 2. Simulated capacitance vs. fluid depth for the no beveled 7 cm applicator. a) Previously designed detector, b) Proposed geometry. The ordinate scales have been selected according to the regions of interest. Dotted lines represent linear fitting. Blue: 0° tilted; Red: 45° (I) tilted, orientation of the applicator towards the gap between the two strips; Yellow: 45° (II) tilted, orientation of the applicator towards the center of the two strips. (For interpretation of the references to colour in this figure legend, the reader is referred to the web version of this article.)

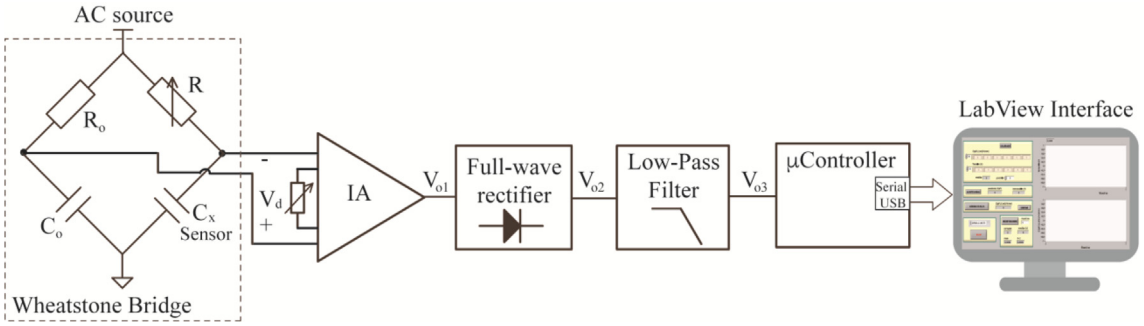

Fig. 3. Block diagram for the measurement circuit, acquisition and monitoring.

2.3. Measurement circuit, acquisition and monitoring

In order to not adversely affect the detection threshold due to the decrease in sensitivity associated with the chosen geometry, we propose a modification of the simple RC reading circuit used in reference [12] to reduce the inaccuracies associated with the reading process.

As the variation of the capacitance to be measured is extremely small (i.e. less than 0.1 pF), the parasitic capacitance of the 80 cm coax cable that connects the sensor with the measurement circuit (i.e. around 100 pF) represents a huge limitation in the accuracy of the measurement. For this reason, a solution based on a differential measurement has been considered.

Fig. 3 shows the block diagram of the measurement circuit. It is based on a Wheatstone Bridge (WB) with alternating current (AC) source and subsequent signal conditioning using an instrumentation amplifier (IA), rectifier and low-pass filtering. The design of the WB-IA pair for the measurement procedure is crucial in term of noise. Indeed, on the one hand the WB allows obtaining a good signal to noise ratio (SNR), extracting exclusively the differential signal of interest. On the other hand, the amplifier stage requires a high common-mode rejection ratio (CMRR) to ensure the amplification exclusively of the differential signal and to eliminate the WB common mode signal. The conditioning circuit works as follows:

The AC source is generated by a frequency-programmable oscillator whose frequency is configured in such a way that the combination formed by the sensor and the connection cable between it and the conditioning circuit (C_x in Fig. 3) is pure capacitive. In this way, only two resistors and two capacitors conform the WB. In our case, for 80 cm cable length, the working frequency is set to 20 kHz.

The design of the WB has been made so that the crossing frequency of the R_o-C_o and R- C_x networks is less than 20 kHz. Therefore, when the fluid level in the applicator increases the attenuation of the R-C_x network also increases, which produces an amount in the SNR of the WB differential output signal (V_d in Fig. 3). Since its amplitude is still extremely low (of the order of mV) an adjustable 10^2–10^3 gain – high CMRR IA is needed.

The effective variable gain (attenuation/amplification) obtained by the WB-IA pair plays an important role in the determination of the detector sensitivity. An increasing in the gain would entail a better sensitivity and therefore the possibility of reducing the threshold detection (obviously, there is a limitation on gain due to saturation of the amplifier). In a similar way, adjusting the WB-IA would allow equalizing the response of the circuit for the different applicator diameters.

The amplitude of V_d is amplified by the IA (V_{o1}) and extracted by a full-wave rectifier (V_{o2} output) followed by a 10 Hz cut-off frequency low-pass filter (V_{o3}). Thus, the result of the conditioning circuit shows a very good proportionality between the fluid present in the applicator and the V_{o3} output signal. The total power consumption of the measurement circuit is lower than 90 mW (5 V, < 18 mA).

Acquisition of V_{o3} signal is performed by means of an internal ADC of a microcontroller that is connected to a PC via USB port. The ADC is working in free-running mode at 10 kHz sampling frequency. Each data acquisition averages the result of 50 ADC samples.

Data acquired is monitored at a rate of 1 Hz by a developed LabView-based graphical interface. By this means, the user can increase the number of samples to be averaged on a run, modify the elapsed time between measurements and monitor the extended uncertainty associated with the measurement. After a run, the depth of fluid accumulated for a given applicator diameter is plotted.

2.4. Setups

To evaluate the detector sensitivity and be able to compare the results obtained in reference [12], an experiment was developed using water simulating blood or any organic fluid, at room temperature (22–24 °C) and for the same setups schemes described in the aforementioned reference.

Three setups based on different applicator diameters are considered, ranging from 4 cm to 10 cm. In this way the entire range of available applicator sizes used with this accelerator is covered. The 4 cm applicator diameter is the smallest one used in the clinic for intraoperative treatment with this accelerator, mainly in the treatment of breast with small target volume. The 10 cm applicator diameter is the largest one used, mainly used in large targets (i.e. sarcomas). The setups are as follows:

Setup 1: 10 cm applicator diameter with no bevel 0° tilted, where the fluid has the same depth along the entire surface and 45° tilted where the fluid is accumulated in a corner.
Setup 2: 7 cm applicator diameter with no bevel 0° tilted and 45° tilted.
Setup 3: 4 cm applicator diameter with no bevel 0° tilted and 45° tilted.

Fig. 4 shows a picture of the implemented prototype (7 cm applicator). The sensor has been manufactured as a two-layer printed circuit board (PCB). The six strips forming a plate are connected together through a very thin copper trace (i.e. 0.5 mm) embedded into a kapton film for an easy manipulation of the PCB-manufactured sensor. The applicator is fixed to a bottom methacrylate plate with a silicone glue layer and the strips are then placed as close to the bottom plate as possible (i.e. 3 ± 1 mm). Visibility through the detector has been chosen to be greater than 50% (i.e. 66%).

In order to simplify the handling of the detector during the development of the tests carried out, the detector has been located on the outer surface of the applicator. Due to the extremely low currents through the detector (< 30 µA rms) no risk associated to electrical shock is considered when manipulating the prototype. However, in view of a future clinical application, a simple modification of the applicator will allow embedding the detector in its lower end thus avoiding any contact with the patient.

For simplicity, the electronics has been developed using standard

Fig. 4. Implemented sensor prototype (7 cm applicator is shown). It can be seen the two sets of six detector sections (12 strips) interspersed with each other and located 3 mm away from the bottom of the methacrylate plate. Strips are 1.5 cm height, 0.5 cm width.

circuitry connected to a commercial power supply. For clinical use, this can be easily miniaturized using low-power surface mounted devices (SMD) circuitry connected to a very small battery and integrated into the applicator or simply connected through the 80 cm cable to the external microprocessor located at the head of the linac.

3. Results

Fig. 5 (setup 1), Fig. 6 (setup 2) and Fig. 7 (setup 3) show the percentage variations of the output voltage (ΔV_{out}) with respect to the zero condition V_0 as a function of the depth of fluid, measured with respect to the horizontal surface. Since in the setups the detector is located 3 mm from the lower end of the applicator fluid depth values are affected by this bias. Therefore, to estimate the actual depth value that would be obtained in the clinical application – in which the detector would be located just at the lower end of the applicator and embedded in it – this 3 mm bias should be subtracted. This is why, the maximum value (1.8 cm) of fluid depth shown in Fig. 5, Fig. 6 and Fig. 7 is the one that equals the height of the sensor measured from the bottom. Vertical dotted lines in Figs. 5–7 show the 0.5 cm ideal detection threshold considered from the beginning of the detector (3 mm from the bottom).

Fig. 5 shows the experimental results for setup 1. The response of the detector against the depth of fluid present in the 10 cm applicator, both for 0° tilted (blue) and 45° tilted (red). Sensitivity is about 38.7 (%)/cm for 0° tilted, and about 10.8 (%)/cm for 45° tilted. The statistically expanded uncertainty is 0.49%, coverage factor k = 2.

Fig. 6 shows the experimental results for setup 2. It can be seen the response of the detector against the depth of fluid present in the 7 cm applicator, both for 0° tilted (blue) and 45° tilted (red). Sensitivity is about 39.6 (%)/cm for 0° tilted, and about 9.7 (%)/cm for 45° tilted. The statistically expanded uncertainty is 0.53%, coverage factor k = 2.

Fig. 7 shows the experimental results for setup 3. It can be seen the response of the detector against the depth of fluid present in the 4 cm applicator, both for 0° tilted (blue) and 45° tilted (red). Sensitivity is about 27.1 (%)/cm for 0° tilted, and about 5.1 (%)/cm for 45° tilted. The statistically expanded uncertainty is 1.46%, coverage factor k = 2.

4. Discussion

The chosen geometry after Comsol Mutiphysics simulations, based on two sets of six strip interspersed with each other, has allowed us to:

i) Reduce the impact of the detector below 50% on the visual through plastic applicators. As seen in Fig. 4, a visibility of 66% is achieved which should be enough for the surgeon to manipulate the applicator without appreciably notice the presence of the detector.
ii) Diminish the asymmetry produced in the detection capability when the applicator is tilted. As shown in Fig. 2, sensitivity for 45° tilted does not depend on the orientation of the fluid, either towards the separation between the capacitor strips or towards the center of the strip. Therefore, the orientation dependence is practically

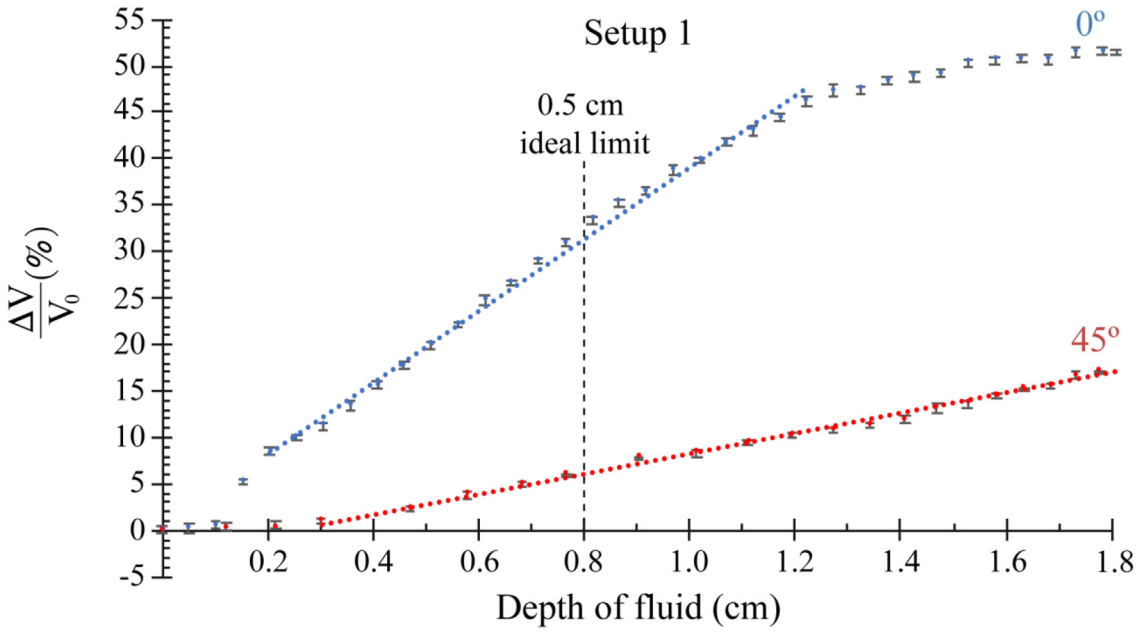

Fig. 5. Percentage variations with respect to the zero condition V_0 vs. the depth of fluid for setup 1 (10 cm applicator diameter). Blue: 0° tilted. Red: 45° tilted. Error bars represent one standard deviation. Dotted lines represent linear fitting. (For interpretation of the references to colour in this figure legend, the reader is referred to the web version of this article.)

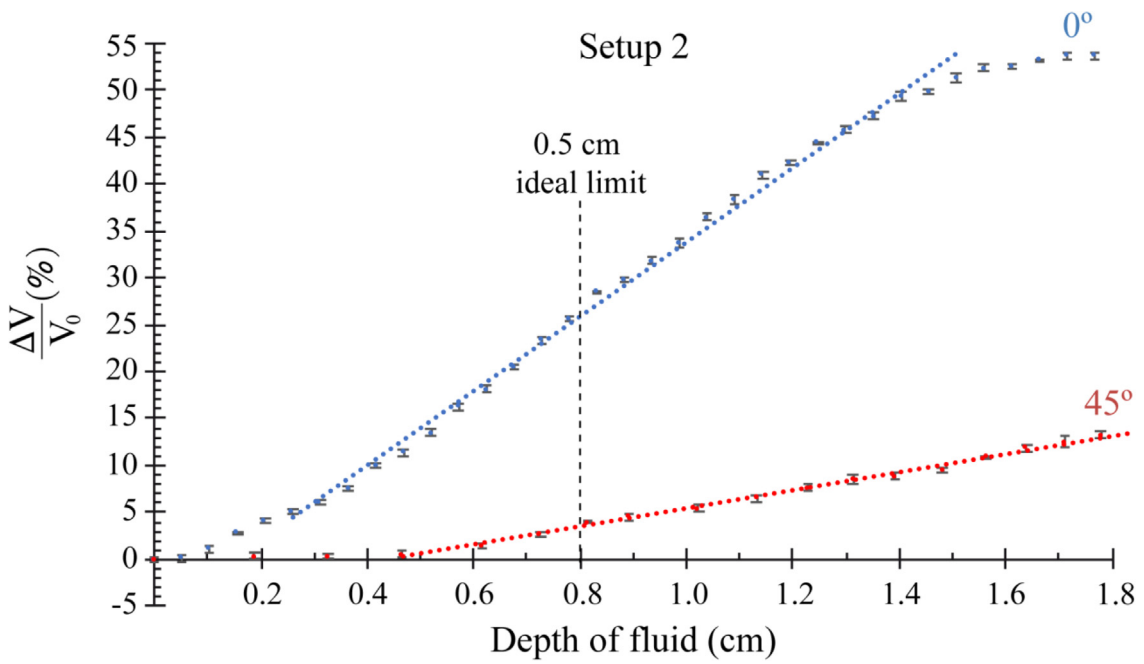

Fig. 6. Percentage variations with respect to the zero condition V_0 vs. the depth of fluid for setup 2 (7 cm applicator diameter). Blue: 0° tilted. Red: 45° tilted. Error bars represent one standard deviation. Dotted lines represent linear fitting. (For interpretation of the references to colour in this figure legend, the reader is referred to the web version of this article.)

eliminated.

The dependence of the sensitivity with the diameter of the applicator has been equalized for setups 1 and 2, by means of the WB-IA stage, as seen in Fig. 5 and Fig. 6. However, since for setup 3 the capacitive variations are extremely low (i.e. 1 fF), adjusting the WB-IA does not allow the entire common mode signal rejection. Therefore, the gain of the IA must be limited to avoid its saturation thus entailing a lower sensitivity. As shown in Fig. 7 this is particularly critic for the 45° tilted which represents the worst-case scenario.

When the applicator is located at 0° we verify that the detection capacity allows to obtain real thresholds clearly below the ideal limit established in 0.5 cm for the three setups. When the applicator is 45° tilted the detection capacity below this limit is still clearly maintained for setups 1 and 2 (diameters 10 cm and 7 cm respectively), although it remains in the limit for setup 3 (diameter of 4 cm). Regarding this last issue, it should be noted that in this case the fluid is accumulated into the corner of the applicator and it is not distributed to its central part. In particular, for a 0.5 cm depth of fluid, which represents volumes lower than 0.6 ml (roughly 10 drops) for any of the three setups, surface ocuppancies in the applicators are lower than 3%, 5% and 9% (for 10 cm, 7 cm and 4 cm applicator diameters, respectively). This very

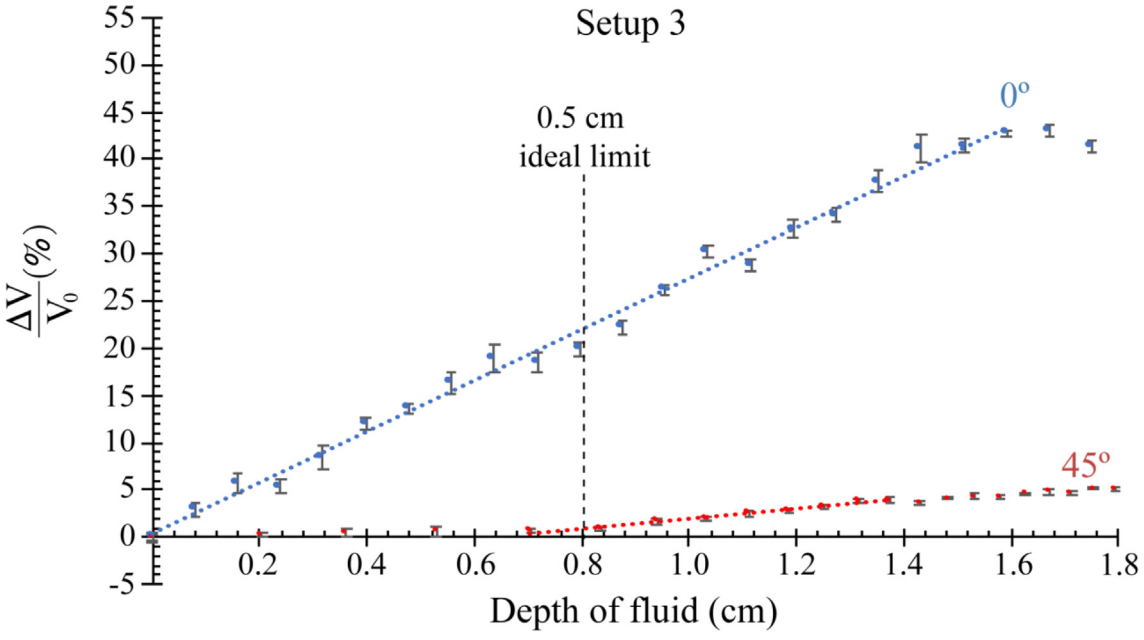

Fig. 7. Percentage variations with respect to the zero condition V_0 vs. the depth of fluid for setup 3 (4 cm applicator diameter). Blue: 0° tilted. Red: 45° tilted. Error bars represent one standard deviation. Dotted lines represent linear fitting. (For interpretation of the references to colour in this figure legend, the reader is referred to the web version of this article.)

small fraction could be considered acceptable from the clinical practice point of view.

Depending on the use of the detector, linearity may play an important role. Even in a simple yes/not application, linearity allows the possibility of continously varying the detection threshold. Besides, a linear behaviour opens the possibility of measuring the amount of fluid present in the applicator, if ever needed. As shown in Fig. 5, Fig. 6 and Fig. 7, the response of the detector is linear for the three setups over most of the range of measurement. Outside these range, nonlinearities come from border effects due to either the absence of detector or to the fluid-air interface (lower and upper part of measurement range, respectively).

Regarding the possible influence of the electromagnetic fields existing in the surgery room over the proposed detector, it should be considered that in the course of the irradiation (approximately 2 min) there are no more equipment than those derived from the monitoring of the patient's vital signs and the anesthesia systems, none of which have any influence on the signal of the bleeding detector. Therefore, no protection, isolation or shielding was considered.

Furthermore, due to the extremely low current circulating through the detector, no electric protection was required in the handling of the equipment, so no danger due to an electric shock was foreseen. Nevertheless, it is clear that the final clinical product should be embedded into the applicator thus avoiding any contact between the detector and the patient.

5. Conclusions

We have designed a new bleeding detector for use in intraoperative radiotherapy that represents an improvement of another one previously developed in our group. This new detector overcomes limitations to that one, fulfilling with feedback received from clinical procedure. It is performed using a low-cost and low-power capacitive sensor copper-PCB kapton based.

The proposed detector uses an interspersed strip geometry to form the two capacitor plates and features the following: i) high visibility through the PMMA applicator (i.e. 66%), as is the case of the ones used in LIAC HWL; ii) non-dependence on the amount of fluid accumulated in the applicator with its orientation, when tilted; iii) high threshold discrimination of fluid, around 0.5 cm even in the worst case scenario; iv) linearity over most of the range of measurement and v) easy to embedded and install. It is important to notice that the proposed improvements for the capacitive bleeding detector do not compromise neither its industralization nor its cost.

The developed system will reduce the uncertainties or dose misadministration events due to the potential bleeding in the post-resected surface. Therefore, the impact of the proposed detector is significant both in terms of quality assurance and outcome of treatment.

The prototype is ready for its industrialization. The whole system can be easily miniaturized and embedded in the lower end of the applicator, so the final clinical product will have no impact on either the structure or the current capabilities of the applicator while avoiding any contact between the detector and the patient.

Acknowledgments

This work is framed in a collaboration agreement between S.I.T Sordina IORT Technologies SpA and University of València-Estudi General. We would like to thank Dr. Giuseppe Felici for his cooperation.

References

[1] Calvo FA, Meirino RM, Orecchia R. Intraoperative radiation therapy. First part: Rationale and techniques. Crit Rev Oncol Hematol 2006;59:106–15. https://doi.org/10.1016/j.critrevonc.2005.11.004.

[2] Valentini V, Calvo F, Reni M, Krempien R, Sedlmayer F, Buchler MW, et al. Intraoperative radiotherapy (IORT) in pancreatic cancer: joint analysis of the ISIORT-Europe experience. Radiother Oncol 2009;91:54–9. https://doi.org/10.1016/j.radonc.2008.07.020.

[3] Kusters M, Valentini V, Calvo FA, Krempien R, Nieuwenhuijzen GA, Martijn H, et al. Results of European pooled analysis of IORT-containing multimodality treatment for locally advanced rectal cancer: adjuvant chemotherapy prevents local recurrence rather than distant metastases. Ann Oncol 2010;21:1279–84. https://doi.org/10.1093/annonc/mdp501.

[4] Van De Voorde L, Delrue L, Van Eijkeren M, De Meerleer G. Radiotherapy and surgery-an indispensable duo in the treatment of retroperitoneal sarcoma. Cancer 2011;117:4355–64. https://doi.org/10.1002/cncr.26071.

[5] Haddock MG, Miller RC, Nelson H, Pemberton JH, Dozois EJ, Alberts SR, et al. Combined modality therapy including intraoperative electron irradiation for locally recurrent colorectal cancer. Int J Radiat Oncol Biol Phys 2011;79:143–50. https://doi.org/10.1016/j.ijrobp.2009.10.046.

[6] Haddock MG. Intraoperative radiation therapy for colon and rectal cancers: a clinical review. Radiat Oncol 2017;12:1–8. https://doi.org/10.1186/s13014-016-0752-1.

[7] Roeder F, Krempien R. Intraoperative radiation therapy (IORT) in soft-tissue sarcoma. Radiat Oncol 2017;12:1–13. https://doi.org/10.1186/s13014-016-0751-2.

[8] Krengli M, Pisani C, Deantonio L, Surico D, Volpe A, Surico N, et al. Intraoperative radiotherapy in gynaecological and genito-urinary malignancies: focus on endometrial, cervical, renal, bladder and prostate cancers. Radiat Oncol 2017;12. https://doi.org/10.1186/s13014-016-0748-x.

[9] Baghani HR, Robatjazi M, Mahdavi SR, Nafissi N, Akbari ME. Breast intraoperative electron radiotherapy: image-based setup verification and in-vivo dosimetry. Phys Medica 2019;60:37–43. https://doi.org/10.1016/j.ejmp.2019.03.017.

[10] Calvo FA. Intraoperative irradiation: precision medicine for quality cancer control promotion. Radiat Oncol 2017;12:1–5. https://doi.org/10.1186/s13014-017-0764-5.

[11] López-Tarjuelo J, Morillo-Macías V, Bouché-Babiloni A, Ferrer-Albiach C, Santos-Serra A. Defining action levels for in vivo dosimetry in intraoperative electron radiotherapy. Technol Cancer Res Treat 2015;15:453–9. https://doi.org/10.1177/1533034615588196.

[12] Sanchis E, Casans S, Felici G, García-Gil R, Sanchis-Sánchez E, Pérez-Calatayud I, et al. Detector for monitoring potential bleeding during electron intraoperative radiotherapy. Phys Medica 2019;57:95–9. https://doi.org/10.1016/j.ejmp.2018.12.010.

[13] LIAC HWL Mobile Ioert Accelerator n.d. https://www.soiort.com/products/liac-hwl/ (accessed October 26, 2018).

[14] Nevelsky A, Bernstein Z, Bar-Deroma R, Kuten A, Orion I. Design and dosimetry characteristics of a commercial applicator system for intra-operative electron beam therapy utilizing ELEKTA Precise accelerator. J Appl Clin Med Phys 2010;11:57–69. https://doi.org/10.1120/jacmp.v11i4.3244.

[15] Gunderson LL, Willett CG, Calvo FAHL. Intraoperative irradiation. Techniques and results. 2th ed. Springer; 2011.

[16] COMSOL. Introduction to COMSOL Multiphysics 2015. http://cdn.comsol.com/documentation/5.1.0.145/IntroductionToCOMSOLMultiphysics.pdf.